SAND2017-7860J
WILEY-VCH

COMMUNICATION

Reversible, Redox-Induced Modulation of Sterics in an α-Diimine Ligand Coordinated to Gallium

Ryan A. Zarkesh,[b] Michael E. Foster,[b] Andrew S. Ichimura,[c] and Mitchell R. Anstey*[a]

Abstract: The ability to tune the steric envelope through redox events post-synthetically or in tandem with other chemical processes is a powerful tool that could assist in enabling new catalytic methodologies and understanding potential pitfalls in ligand design. The α-diimine ligand, dmp-BIAN, exhibits the peculiar and previously unreported feature of varying steric profiles depending on oxidation state when paired with a main group element. A study of the factors that give rise to this behaviour as well as its impact on the incorporation of other ligands is performed.

Steric crowding of metal center is used to control coordination number, substrate-catalyst selectivity, stability of unusual bonding modes, and even redox processes.[1-7] The literature relating to steric effects is rich and varied, but steric effects are typically a static factor that is determined at the molecular design stage. Post-synthetic modifications of metal complexes exist,[8-10] but these stoichiometric processes can be incompatible with other parallel reactions. In other words, changing the steric profile of a ligand during an ongoing chemical process is a difficult task.

Some interesting examples of steric augmentation either post-synthetically or in tandem with other chemical processes include photoisomerization of azobenzenes and metal-ligand complexes,[11-13] pH-switchable rotaxanes and ruthenium NHCs,[14,15] and ion- or ligand-selective coordination complexes.[16,17] Redox-switchable compounds are another route for expanding functionality,[18] and recent reports have demonstrated the efficacy of ferrocenyl-type ligands and metal-center redox changes inducing "on/off" catalytic reactivity.[19-25] However, these latter systems do not change sterics and operate mostly through modulation of Lewis acidity/basicity or solubility.

Redox-active ligands create the possibility for ligand-only reactivity that can adjust the steric environment around the metal center.[26-29] Two general archetypes for this process include a reduction or oxidation process that (1) causes a movement of the ligand to shield or reveal a binding site on a metal center or (2) creates or removes degrees of freedom or flexibility that shield a binding site on the metal center (Figure 1). Our group began exploring this concept in the context of redox-active ligands paired with main group elements for battery applications.[30] A competent battery electrolyte should maintain stability through thousands of redox cycles, and a metal-based electrolyte with a protected inner coordination sphere should remain viable for longer, increasing the lifespan of the battery.[31-33]

Our efforts have focused on the α-diimine ligand family due to its ease of synthesis, numerous potential structural combinations, and wealth of existing knowledge on electrochemical properties.[34-41] *N*, *N*′-bis(3,5-dimethylphenylimino)acenaphthene (dmp-BIAN) is one example of an intermediate sterically crowded α-diimine ligand (Figure 2), and both 4- and 6-coordinate gallium complexes have been isolated in our laboratory. In the course of this work, an interconversion process between these two complexes was discovered that appears to be controlled by a reversible redox-induced change in the steric envelope of the ligand; a process that has not been previously described. What follows is an investigation into the mechanism of this redox-mediated process.

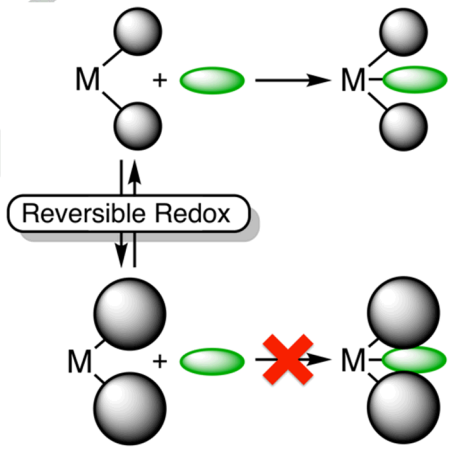

Figure 1. Reversible redox process localized on a coordinated ligand changes the steric envelope of that ligand and the resulting reactivity of the complex.

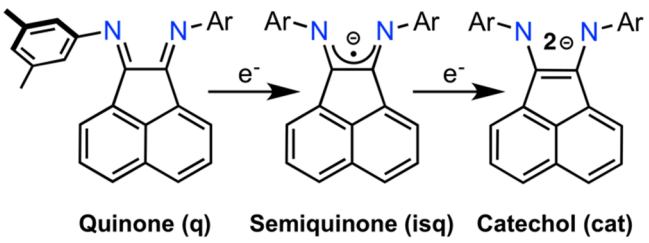

Figure 2. Oxidation states of dmp-BIAN ligand (Ar = 3,5-dimethylphenyl).

Ready access to the neutral Ga(dmp-BIAN^{isq})(dmp-BIAN^{cat}) complex, **1**, is obtained by heating solutions of dmp-BIAN^{q} ligand and gallium/mercury amalgam in tetrahydrofuran (THF) at 60°C for 24 h (Scheme 1). The resulting dark blue solutions are filtered, concentrated under vacuum, and then layered with excess hexanes to afford the desired product as a dark blue

[a] Prof. Dr. M. R. Anstey
Department of Chemistry
Davidson College, Box 7120 Davidson, NC 28035, USA.
E-mail: mianstey@davidson.edu
[b] Dr. R. A. Zarkesh and Dr. M. E. Foster
Sandia National Laboratories, P.O. Box 969 MS 9292, Livermore, CA 94551, USA.
[c] Prof. Dr. A. S. Ichimura
Department of Chemistry & Biochemistry, San Francisco State University, 1600 Holloway Avenue, San Francisco, CA 94132, USA.

Supporting information for this article is given via a link at the end of the document.

microcrystalline solid in 90% yield. The 6-coordinate complex Ga(dmp-BIAN^{isq})$_3$, **2**, is obtained in a similar fashion using a 3:1 molar ratio of reactants, yielding a red microcrystalline solid (Scheme 1).[4]

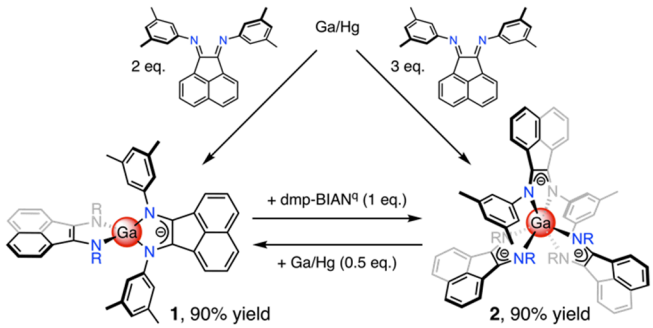

Scheme 1. Synthesis and interconversion between Ga(dmp-BIAN^{isq})(dmp-BIAN^{cat}), **1**, and Ga(dmp-BIAN^{isq})$_3$, **2**.

According to X-ray diffraction studies, the gallium center of **2** is in a distorted octahedral environment with the three BIAN ligands placed in a *D*$_3$ symmetric arrangement about the metal center (Figure 3A and 3B). Based on previous magnetic susceptibility, EPR, and structural metrics, the ligands are in the semiquinonate oxidation state with the α-diimine backbone adopting a planar geometry extending through the *ipso* carbons of each appended aryl group.[30] These results are in agreement with the characteristics of related α-diimine complexes.[42-44]

The structure of the neutral 4-coordinate complex, **1**, differs substantially in both electronics and sterics (Figure 3C and 3D). The two BIAN ligands are in a distorted tetrahedral arrangement about the gallium center and show two sets of C–N bond lengths: 1.405(2) Å and 1.395(2) Å, 1.337(2) Å and 1.343(2) Å. These bond lengths suggest that the BIAN ligands are in a mixed valent state (i.e. dmp-BIAN^{isq} and dmp-BIAN^{cat}). Further evidence of the two different oxidation states can be seen in the C–C bond lengths (C1–C2, 1.374(3) Å and C29–C30, 1.442(3) Å). Finally, the gallium-nitrogen bond lengths are shorter for the catecholate ligand compared to the semiquinonate ligand. The semiquinonate ligand adopts a planar structure similar to the BIAN ligands in **2**, but the catecholate shows a substantial deviation from planarity. With the α-diimine backbone as the reference plane, one aryl group is angled approximately 44° out of plane. All crystal structures of this compound obtained in our laboratory, regardless of the method used, show a substantial deviation from planarity. While it is possible that this deviation is due to packing forces within the crystal, it is also consistent with the catecholate oxidation state of the ligand. As the ligand is reduced from semiquinonate to catecholate, the geometry at nitrogen is pyramidalized due to an increase in electron density partially localized on the atom. This difference in structure based on the ligand's oxidation state underpins the following results.

In our hands, this and a related 4-coordinate complex (*vide infra*) can only be isolated when at least one BIAN ligand is in the doubly-reduced, catecholate oxidation state. Furthermore, if that oxidation state is maintained, the complexes will not incorporate a third ligand. The addition of pyridine, dimethylformamide, 9,10-phenanthrenequinone, 1,10-phenanthroline, 2,2'-bipyridine, or 2-(phenyliminomethyl)pyridine to **1** gave no new heteroleptic 6-coordinate complexes. However, the addition of one equivalent of dmp-BIAN^{q} to **1** affords complex **2** in quantitative yield (Scheme 1). Conversely, stirring complex **1** in the presence of additional fresh gallium amalgam regenerated complex **2** in high yields (>90%, Scheme 1).

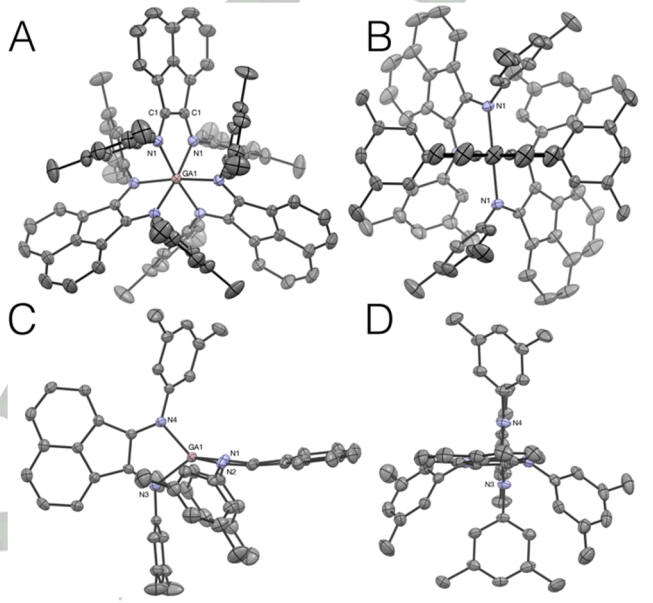

Figure 3. A) Structural diagram of **2** with ellipsoids drawn at 50% probability. B) Side view of **2**. C) Structural diagram of **1** with ellipsoids drawn at 50% probability. D) View of **1** along the BIAN ligand backbone. All hydrogen atoms, and solvent molecules have been omitted for clarity.

It is important to note that both of these conversions must be accompanied by some electron transfer process. Literature references show that the reduction potential of dmp-BIAN^{q}[40] is the most positive of all of the aforementioned ligand candidates.[45-48] Our working hypothesis at this point was that the incorporation of a third ligand must coincide with an oxidation of all catecholate BIAN ligands to the semiquinonate.

The cyclic voltammogram of **1** recorded in THF (-1.3 V to -0.6 V) shows a quasi-reversible reduction event that persists for at least 5 cycles (see Supporting Information). However, cycling over a larger voltage window (-1.3 V to +0.8 V) shows rapid decomposition (Figure 4, top). The same experiment performed in pyridine solution resolves into a pair of quasi-reversible peaks at -0.83 V and -0.40 V (Figure 4, middle). If the CV experiment in THF is repeated with 6 equivalents of 2,2'-bipyridine, the CV resolves into a set of 3 quasi-reversible peaks, notably similar in behaviour to the observations of the pyridine solution (Figure 4, bottom).

Guided by these results, it was reasoned that (1) complex **1** could be reduced stoichiometrically to the monoanion and (2) complex **1** could be oxidized in the presence of coordinating ligands to form new heteroleptic complexes.

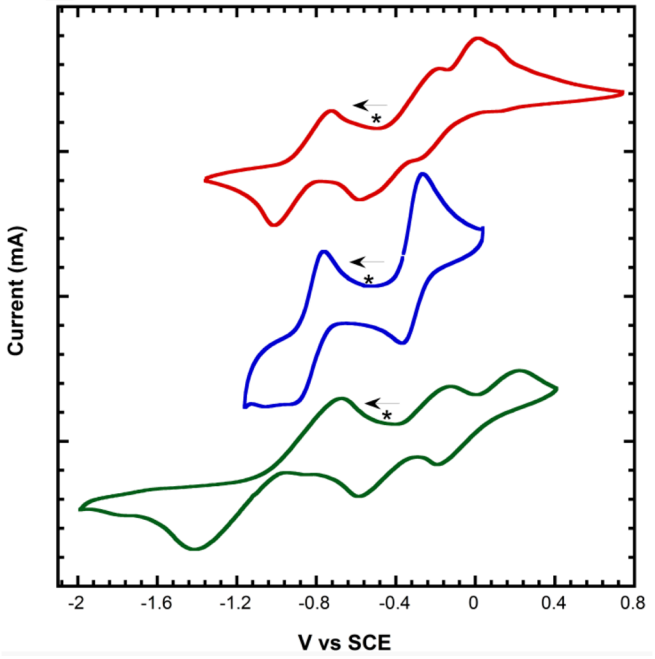

Figure 4. Cyclic voltammograms of **2** in THF (red), pyridine (blue), and in THF with 6 equivalents of 2,2′-bipy (green). Measurements were made under N_2 using a scan rate of 200 mVs^{-1} in 3 mM solutions containing 0.1 M $LiPF_6$ electrolyte. Potentials were referenced to SCE using the $Cp_2Fe^{0/+}$ couple as an internal standard ($Cp_2Fe^{0/+}$= 0.58 V vs SCE in THF; $Cp_2Fe^{0/+}$= 0.72 V vs SCE in pyridine). Asterisks indicate starting point for each scan, and the arrows indicate the initial direction.

Reduction of complex **1** with one equivalent of Cp_2Co or potassium metal affords the closed shell monoanion [Ga(dmp-BIAN^{cat})$_2$][Cp_2Co], **3a,** (Scheme 2) in 85% yield as a dark blue microcrystalline solid after recrystallization from THF/hexanes. The potassium salt can be generated by reducing **1** with excess potassium metal and recrystallizing from a Et_2O/THF (5/1 v/v) solvent mixture. The crystal structures of **3a** and **3b** show both ligands deviating from planarity similar to that of complex **1**. In the case of **3a** and **3b**, we have observed two types of structural isomers in the solid state for each complex depending on crystallization conditions (Figure 5). Either the 3,5-dimethylphenyl substituents are staggered above and below the plane of the acenaphthene (Figure 5A) or they form a “syn” conformation arching to the same side (Figure 5B). In contrast to the structural data, NMR analysis of [Ga(dmp-BIAN^{cat})$_2$][K•(Et_2O)$_3$], **3b**, reveals a *C*2$_v$ symmetric complex in solution based on the observation of only one set of aryl-methyl peaks at 2.16 ppm (see Supporting Information). This symmetry can only be possible if the amines are able to invert rapidly on the time scale of the NMR experiment.

To support this rationalization, Density Functional Theory calculations were performed to determine the energy barrier to inversion. With the crystallographic data of **1** as a starting point, one nitrogen of the catecholate was forced through the assumed inversion process to map out the potential energy curve (Figure 6). The highest point in energy (the presumed transition state) coincides with the nitrogen in a planar orientation, and the two local minima correspond to a +/- 40° bend in the dihedral angle away from planar. Depending on the orientation of adjacent aryl groups, it was found that the kinetic barrier could be either 6.1 or 3.2 kcal/mol. The deeper energy well appears to be enabled by π-π stacking. In either case, this energy barrier matches well with free trialkyl amines,[49,50] meaning a rapid inversion of the catecholate BIAN nitrogen is possible.

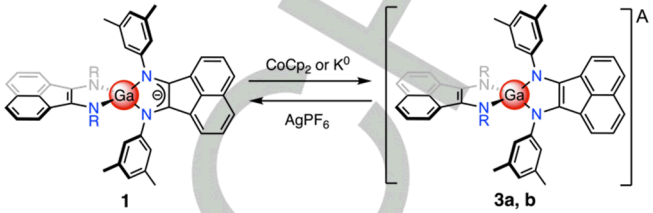

Scheme 2. Reduction of **1** to **3a** or **3b** (3a, A = Cp_2Co^+; 3b, A = K^+•(Et_2O)$_3$). Reoxidation with silver hexafluorophosphate also pictured.

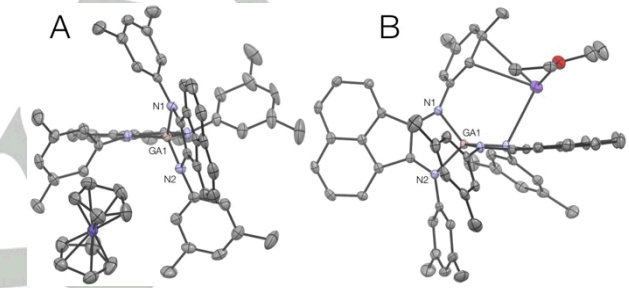

Figure 5. A) Structural diagram of **3a** with ellipsoids drawn at 50% probability. B) Structural diagram of **3b** with ellipsoids drawn at 50% probability.

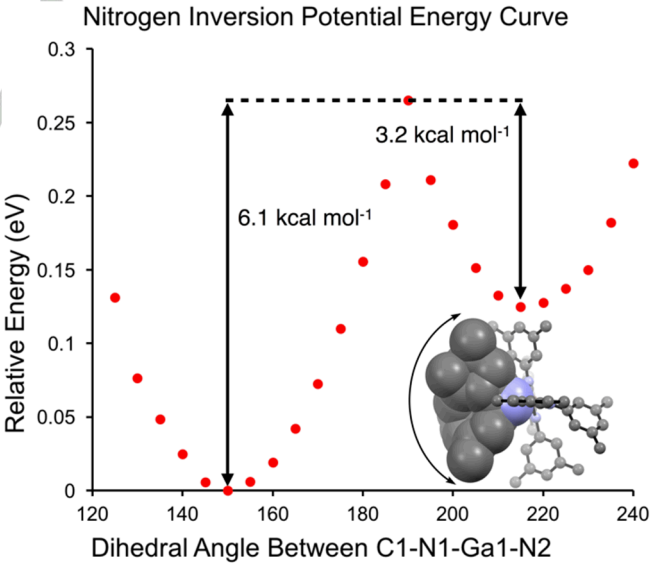

Figure 6. Graph of potential energy curve through the nitrogen inversion process of complex **1**. Inset is the overlaid full “range of motion” from 150° to 215° along the dihedral angle of C1-N1-Ga1-N2.

Putting these observations together, it is likely that the catecholate oxidation state is enabling increased flexibility at

nitrogen (inversion), and this increased flexibility allows for greater steric protection of the metal center than the dmp-BIAN^{isq} can offer. This steric protection allows for the isolation of low-coordinate complexes that would not necessarily be predicted based on the sterics of the dmp-BIAN moiety itself, especially in light of the fact that complex **2** can be isolated in high yields

When complex **1** is treated with one equivalent of $AgBPh_4$ in the presence of excess 2,2'-bipyridine (Scheme 3, middle), a microcrystalline red solid is obtained after recrystallization (85% yield). X-ray crystallographic studies determined the structure to be that of [Ga(dmp-BIAN^{isq})$_2$(bipy)][BPh_4], **4**. The cyclic voltammogram of this species matches that of the *in situ* electrochemical experiment described above (see Supporting Information). As previously mentioned, bipyridine could not be incorporated without an oxidant or an electrochemical oxidation process.

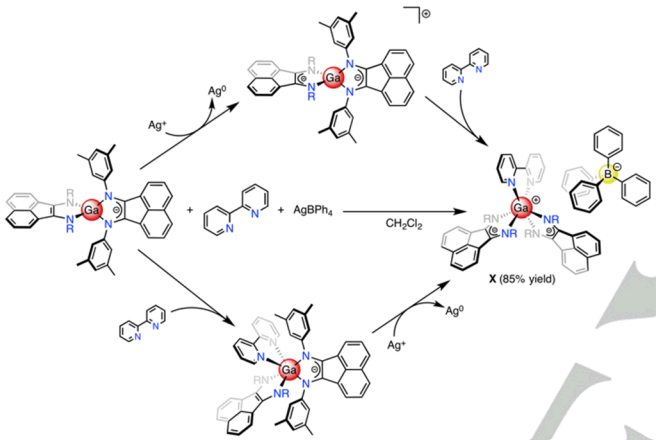

Scheme 3. Synthesis of **4** with two proposed mechanisms: pre-oxidation followed by coordination (top), pre-coordination followed by oxidation (bottom).

These assumptions about sterics due to inversion at nitrogen should hold in the reverse direction as well. Reduction of the heteroleptic cation **4** with one equivalent of Cp_2Co yields a modest amount of **3a** (40% yield). However, treating a solution of **4** with two equivalents of Cp_2Co results in the clean isolation of **3a** after recrystallization (85% yield). Subjecting **2** to the same reduction reaction conditions gives the same product in almost identical yield ruling out any unique effect imparted by bipyridine. From a mechanistic standpoint, one semiquinonate ligand will be reduced to the catecholate enabling nitrogen inversion and breaking planarity. The effective steric envelope around that ligand will increase, and a different ligand is lost due to the increased steric crowding at the metal center. Related to these results, the neutral complex **1** can be accessed in high yield after recrystallization (90%) by mixing equimolar amounts of **4** and **3a**.

Buried volume calculations[51-54] were performed using both the crystallographic and computational data to show that the nitrogen inversion process can lead to a larger steric envelope. These calculations examine a sphere surrounding the central metal atom and determine the percentage of this sphere that is blocked or "buried" by coordinated ligands. A single dmp-BIAN^{isq} ligand (specifically, one found in compound **2**) will only block 37.4% of the coordination sphere. We then overlaid and combined three separate computationally-derived dmp-BIAN^{cat} structures (dihedral angles of 150°, 190°, and 220°) to represent the total volume that is shielded by a aryl group attached to an rapidly-inverting nitrogen atom. This combined structure gave a buried volume of 51.8%, aligning with our hypothesis that a flexibile dmp-BIAN^{cat} ligand has a dramatically increased steric envelope and can hinder the coordination of a third ligand.

Proper ligand selection to account for both steric bulk and electronic properties is key to developing the ideal catalyst. Battery electrolytes are also subject to structural and electronic factors to impart stability and therefore, applicability. The authors believe that the pairing of a redox-active ligand with a main group element in this way have created the ideal environment to observe differential reactivity based on ligand oxidation states. In this case, the nitrogens in dmp-BIAN^{cat} are allowed increased flexibility through inversion, increasing the effective steric bulk of the ligand. Oxidation to the semiquinonate opens up the coordination sphere to new incoming ligands by reverting the nitrogens back to a planar orientation. The authors believe that other systems like this likely exist, and these effects are not unique to α-diimine ligands. It is hoped that new ligand systems can create dynamic environments for catalyst-substrate specificity, enhancing structural integrity of battery electrolytes, and the isolation of exotic and compelling species to expand our understanding of chemical structure.

Acknowledgements

The authors would like to acknowledge Prof. Neil Tomson (Pennsylvania), Prof. W. Hill Harman (UC Riverside), and Prof. David Blauch (Davidson) for their guidance and helpful conversations over the course of this work. The authors would like to thank Dr. Imre Gyuk; the U. S. Department of Energy, Office of Electricity Delivery and Energy Reliability (Energy Storage Program); and Davidson College for financial support. Sandia National Laboratories is a multi-program laboratory operated by Sandia Corporation, a wholly owned subsidiary of Lockheed Martin Company, for the U. S. Department of Energy's National Nuclear Security Administration under contract DE-AC04-94AL85000.

Keywords: non-innocent ligand • steric hindrance • gallium • nitrogen inversion

[1] S. T. Haubrich, P. P. Power, *J. Am. Chem. Soc.* **1998**, *120*, 2202–2203.
[2] P. Vasko, S. Wang, H. M. Tuononen, P. P. Power, *Angew. Chem. Int. Ed.* **2015**, *54*, 3802–3805.
[3] R. H. Crabtree, *New J. Chem.* **2011**, *35*, 18–23.
[4] R. C. Fischer, P. P. Power, *Chem. Rev.* **2010**, *110*, 3877–3923.
[5] Y. Mizuhata, T. Sasamori, N. Tokitoh, *Chem. Rev.* **2009**, *109*, 3479–3511.
[6] P. P. Power, *J. Organomet. Chem.* **2004**, *689*, 3904–3919.
[7] L. Gonsalvi, J. A. Gaunt, H. Adams, A. Castro, G. J. Sunley, A. Haynes, *Organometallics* **2003**, *22*, 1047–1054.
[8] Z. Wang, S. M. Cohen, *Chem. Soc. Rev.* **2009**, *38*, 1315–

1329.
[9] K. K. Tanabe, S. M. Cohen, *Chem. Soc. Rev.* **2011**, *40*, 498–519.
[10] C. Janiak, J. K. Vieth, *New J. Chem.* **2010**, *34*, 2366–2388.
[11] A. J. Teator, D. N. Lastovickova, C. W. Bielawski, *Chem. Rev.* **2016**, *116*, 1969–1992.
[12] A. Ueno, K. Takahashi, T. Osa, *J. Chem. Soc., Chem. Commun.* **1980**, 837–838.
[13] D. Zhao, T. M. Neubauer, B. L. Feringa, *Nat. Commun.* **2015**, *6*, 6652.
[14] U. Lüning, *Angew. Chem. Int. Ed.* **2012**, *51*, 8163–8165.
[15] K. Arumugam, C. D. Varnado Jr., S. Sproules, V. M. Lynch, C. W. Bielawski, *Chem. Eur. J.* **2013**, *19*, 10866–10875.
[16] H. J. Yoon, J. Kuwabara, J.-H. Kim, C. A. Mirkin, *Science* **2010**, *330*, 66–69.
[17] S. Shinkai, K. Kameoka, K. Ueda, *J. Am. Chem. Soc.* **1987**, *109*, 923–924.
[18] C. G. Oliveri, N. C. Gianneschi, S. T. Nguyen, C. A. Mirkin, C. L. Stern, Z. Wawrzak, M. Pink, *J. Am. Chem. Soc.* **2006**, *128*, 16286–16296.
[19] S. Mortezaei, N. R. Catarineu, J. W. Canary, *J. Am. Chem. Soc.* **2012**, *134*, 8054–8057.
[20] C. K. A. Gregson, V. C. Gibson, N. J. Long, E. L. Marshall, P. J. Oxford, A. J. P. White, *J. Am. Chem. Soc.* **2006**, *128*, 7410–7411.
[21] M. Nishikawa, Y. Takara, Y. Hattori, K. Nomoto, T. Kusamoto, S. Kume, H. Nishihara, *Inorg. Chem.* **2013**, *52*, 8962–8970.
[22] E. M. Broderick, N. Guo, T. Wu, C. S. Vogel, C. Xu, J. Sutter, J. T. Miller, K. Meyer, T. Cantat, P. L. Diaconescu, *Chem. Commun.* **2011**, *47*, 9897–9899.
[23] C. S. Slone, C. A. Mirkin, G. P. L. Yap, I. A. Guzei, A. L. Rheingold, *J. Am. Chem. Soc.* **1997**, *119*, 10743–10753.
[24] I. M. Lorkovic, R. R. Duff Jr., *J. Am. Chem. Soc.* **1995**, *117*, 3617–3618.
[25] S. Ibáñez, M. Poyatos, L. N. Dawe, D. Gusev, E. Peris, *Organometallics* **2016**, *35*, 2747–2758.
[26] V. Lyaskovskyy, B. de Bruin, *ACS Catal.* **2012**, *2*, 270–279.
[27] W. Kaim, *Eur. J. Inorg. Chem.* **2012**, 343–348.
[28] O. R. Luca, R. H. Crabtree, *Chem. Soc. Rev.* **2013**, *42*, 1440–1459.
[29] K. M. Clark, J. W. Ziller, A. F. Heyduk, *Inorg. Chem.* **2010**, *49*, 2222–2231.
[30] R. A. Zarkesh, A. S. Ichimura, T. C. Monson, N. C. Tomson, M. R. Anstey, *Dalton Trans.* **2016**, *45*, 9962–9969.
[31] B. R. Chalamala, T. Soundappan, G. R. Fisher, M. R. Anstey, V. V. Viswanathan, M. L. Perry, *Proc. IEEE* **2014**, *102*, 976–999.
[32] M. H. Chakrabarti, R. A. W. Dryfe, E. P. L. Roberts, *Electrochim. Acta* **2007**, *52*, 2189–2195.
[33] W. Wang, Q. Luo, B. Li, X. Wei, L. Li, Z. Yang, *Adv. Funct. Mater.* **2013**, *23*, 970–986.
[34] I. L. Fedushkin, O. V. Markina, A. N. Lukoyanov, A. G. Morozov, E. V. Baranov, M. O. Maslov, S. Y. Ketkov, *Dalton Trans.* **2013**, *42*, 7952–7961.
[35] I. L. Fedushkin, A. A. Skatova, V. A. Chudakova, G. K. Fukin, *Angew. Chem. Int. Ed.* **2003**, *42*, 3294–3298.
[36] I. L. Fedushkin, O. V. Maslova, A. G. Morozov, S. Dechert, S. Demeshko, F. Meyer, *Angew. Chem. Int. Ed.* **2012**, *51*, 10584–10587.
[37] D. A. Razborov, A. N. Lukoyanov, V. M. Makarov, M. A. Samsonov, I. L. Fedushkin, *Russ. Chem. Bull.* **2015**, *64*, 2377–2385.
[38] H. Schumann, M. Hummert, A. N. Lukoyanov, I. L. Fedushkin, *Organometallics* **2005**, *24*, 3891–3896.
[39] J. Kovach, M. Peralta, W. W. Brennessel, W. D. Jones, *J. Mol. Struct.* **2011**, *992*, 33–38.
[40] K. Hasan, E. Zysman-Colman, *J. Phys. Org. Chem.* **2013**, *26*, 274–279.
[41] J. Bendix, K. M. Clark, *Angew. Chem. Int. Ed.* **2016**, *55*, 2748–2752.
[42] I. L. Fedushkin, V. M. Makarov, V. G. Sokolov, G. K. Fukin, *Dalton Trans.* **2009**, *0*, 8047–8053.
[43] M. M. Khusniyarov, K. Harms, O. Burghaus, J. Sundermeyer, *Chem. Ber.* **2006**, *2006*, 2985–2996.
[44] H. M. Tuononen, A. F. Armstrong, *Dalton Trans.* **2006**, *21*, 1885–1894.
[45] T. Fuchigami, S. Inagi, M. Atobe, Eds., *Fundamentals and Applications of Organic Electrochemistry: Synthesis, Materials, Devices*, Wiley, West Sussex, **2015**.
[46] K. B. Wiberg, T. P. Lewis, *J. Am. Chem. Soc.* **1970**, *92*, 7154–7160.
[47] B. J. Tabner, J. R. Yandle, *J. Chem. Soc., A* **1968**, *0*, 381–388.
[48] P. H. Given, M. E. Peover, *J. Chem. Soc.* **1960**, *0*, 385–393.
[49] A. M. Halpern, M. J. Ondrechen, L. D. Ziegler, *J. Am. Chem. Soc.* **1986**, *108*, 3907–3912.
[50] G. W. Koeppl, D. S. Sagatys, G. S. Krishnamurthy, S. I. Miller, *J. Am. Chem. Soc.* **1967**, *89*, 3396–3405.
[51] A. Poater, B. Cosenza, A. Correa, S. Giudice, F. Ragone, V. Scarano, L. Cavallo, *Eur. J. Inorg. Chem.* **2009**, *2009*, 1759–1766.
[52] A. Poater, F. Ragone, R. Mariz, R. Dorta, L. Cavallo, *Chem. Eur. J.* **2010**, *16*, 14348–14353.
[53] L. Falivene, R. Credendino, A. Poater, A. Petta, L. Serra, R. Oliva, V. Scarano, L. Cavallo, *Organometallics* **2016**, *35*, 2286–2293.
[54] A. Poater, F. Ragone, S. Giudice, C. Costabile, R. Dorta, S. P. Nolan, L. Cavallo, *Organometallics* **2008**, *27*, 2679–2681.

Entry for the Table of Contents (Please choose one layout)

Layout 1:

COMMUNICATION

Text for Table of Contents

((Insert TOC Graphic here))

*Author(s), Corresponding Author(s)**

Page No. – Page No.

Title

Layout 2:

COMMUNICATION

((Insert TOC Graphic here))

*Author(s), Corresponding Author(s)**

Page No. – Page No.

Title

Text for Table of Contents